Anisotropy Characterization of Asymmetric Glass/Epoxy Composites

L.R. Holmes, Jr,
Materials Engineer
U.S. Army Research Laboratory
4600 Deer Creek Look
Aberdeen Proving Grounds, MD, USA 21005

J.M. Considine
Materials Research Engineer
US Forest Service, Forest Products Laboratory
One Gifford Pinchot Drive
Madison, WI, USA 53726

F. Pierron
Professor
University of Southampton
Southampton SO17 1BJ, UK

K.T. Turner
Associate Professor
University of Pennsylvania
245 Towne Building
220 S. 33rd St
Philadelphia, PA, USA, 19104-6315

ABSTRACT

Fast, accurate stiffness identification is a critical component in programs integrating material processing science and mechanical characterization with end-use applications. Variation of material processing parameters coupled with an understanding of the manner in which those variations affect mechanical properties can be used to create a design envelope for customized material development. This work describes a unique load frame designed to produce sufficient full-field strains for identification of all in-plane Q_{ij} from a single test. Surface strains were measured with DIC and processed using a VFM analysis extended to include Q_{16} and Q_{26} identification. Two glass/epoxy composites were examined; one of the materials was intentionally fabricated with a small amount of anisotropy. Quality of stiffness identification was determined. Identified Q_{ij} compared favorably with those calculated by ply-laminate theory.

Keywords: VFM, DIC, stiffness, glass/epoxy, anisotropy

Introduction

Lightweight ground combat vehicles, marine bodies, and aircraft structures using advanced fabric/textile composites and/or layered material architecture are vital because they offer improved deployability, survivability, and agility [1]. The increased need for lightweight materials has amplified the importance of performance evaluations due to the lack of historical databases on new material development efforts. Components, such as the front and rear upper and lower hull, crew capsule, rear-engine bulkhead, ramp, and sidewalls utilize composites with various types of fabric architectures and resin compositions as monocoque or sandwich hybrid constructions [1, 2, 3]. Delamination damage due to ballistic, high strain rate, and intermediate velocity impacts are

critical in most composite structural parts. In addition, many composite structures used in U.S. Army applications are subjected to severe fatigue-loading conditions and harsh environments over long periods of time. Their life and performance depend on fatigue damage tolerance and the rates of property degradation under cyclic or pulse loads [4, 5].

The US Army Research Laboratory (ARL) has a large investment in understanding the life cycle of fiber reinforced polymer (FRP) composites and develops methods to integrate material processing science and mechanical characterization of composite laminate fabrication with end-use applications in mind. It has been proposed that the design envelope offered by a single material system type could be expanded by manipulating material properties through processing. Stiffness being the key material parameter targeted here, the significance of which is best appreciated in the context of system design wherein competing requirements like trade space and energy absorption must be considered.

Within this research, several techniques were developed in order to manipulate stiffness parameters through adjustments in processing making a single material system useful for multiple end-uses [6]. When stiffness is the driving factor in laminate fabrication, repeatability must be proven. Therefore, mechanical evaluation must be fed back into the process engineering component. There are many factors that can contribute to stiffness changes during the life cycle of a laminate, such as: transverse, intralaminar matrix cracking, with or without end delamination; interlaminar matrix cracking; delamination; ply isolation (from combination delaminating and matrix cracking); ply splitting; fiber pull-out; fiber fracture; and others [7]. Because of the multiple failure modes that may occur in this type of evaluation, experimental validation is expensive and time consuming.

In an effort to reduce these costs, we have employed the VFM (Virtual Fields Method) with a specially designed load fixture to evaluate the anisotropic Q_{ij} of two flat FRP composite materials, one orthotropic and one anisotropic. Specimens were subjected to multi-axial loading, within the specimen plane, and surface strain was captured using DIC (digital image correlation). These full-field strains, along with applied force magnitudes, orientations and locations were used in a VFM analysis for stiffness identification. Criteria were developed to ensure identification accuracy. Identified stiffnesses were compared to calculations based on ply-laminate theory.

Materials

For validation of this technique, we have chosen a material system that is commonly processed for Army applications. The reinforcement in the composite laminate is Owens Corning 6781 S-2 glass, which is an 8 harness satin weave of 295 g/m^2, using 9μ 66 tex twisted glass yarns made of magnesium alumino-silicate. These particular yarns are SCG75 1/0 1.0z 636 S-2 glass® yarn. This is a structural and impact resistant material having tensile and flexural values 30-35% higher than E glass fibers. Material properties are shown in Table 1.

Table 1: Manufacturer information for the 6781 S-2 glass reinforcement from [8]

ASTM D1505 Density g/cm^3	Refractive Index	Softening Point °C	Strain Point °C	Sp. Heat Capacity J/g/°C	Thermal Exp. Coef. ppm°C	Dielectric Strength
2.48	1.521-1.525	1056	766	0.737	1.6	13.0

The fiberglass reinforced laminates were fabricated using SC-15 (Applied Poleramic Inc., Benicia, CA) low viscosity epoxy resin system designed for Vacuum Assisted Resin Transfer Molding (VARTM) processing of structural and ballistic composites [9]. The VARTM process results in distinct tool side and bag side surfaces that differed in flatness and roughness. The bag side was consistently used as the observation side during testing. Approximately 95 kPa below standard atmospheric pressure or the equivalent 97 kPa of pressure was achieved in the vacuum bag during processing of the laminates fabricated by this process. A vacuum drop test was performed for one minute using an inline pressure gauge with the vacuum source, demonstrating no greater than 10 kPa pressure change in the vacuum bag. A redundant second vacuum bag was applied over the entire layup to further protect against leaks and decrease potential process variability across the sample set. The VARTM process is illustrated in Figure 1. For a complete overview of the VARTM process, see Rigas et al. [10].

After fabrication, the specimens were machined to final dimensions via computer controlled water jet, thereby eliminating unnecessary thermal or cyclic loadings associated with traditional sawing, milling, or drilling. An auto-generated dot pattern, used for DIC testing, was inkjet printed onto a thin film with adhesive backing and applied to the specimens.

Table 2 shows calculated Q_{ij} for the two materials in this work, where individual ply Q_{ij} are from historical ARL data. Material O is an orthotropic material and Material A is an anisotropic material. The materials have identical plies except that the center ply for Material A has been intentionally rotated 15° to produce non-zero Q_{16} and Q_{26}.

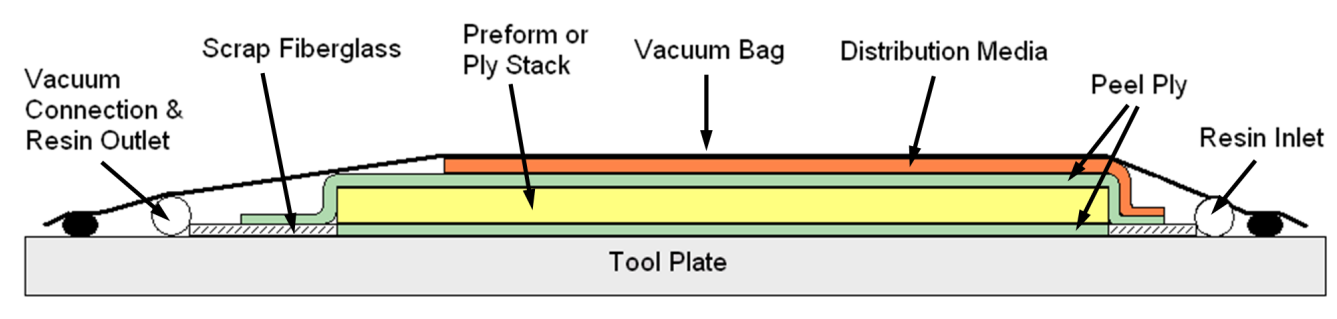

Figure 1: Schematic showing the side view of a composite plate being fabricated by the VARTM process [8].

Table 2: Calculated Q_{ij} from ply lay-up models for orthotropic material, O, and anisotropic material, A. Units (GPa)

Material	Layup	Reference	Q_{11}	Q_{22}	Q_{12}	Q_{66}	Q_{16}	Q_{26}
O	$[0\text{-}90]_3$	[11]	27.84	27.84	3.06	2.90	N/A	N/A
		[12]	31.00	31.00	6.22	2.90	N/A	N/A
A	[0-90/15-105/0-90]	[11]	27.04	27.04	3.85	3.69	1.37	-1.37
		[12]	30.21	30.21	7.01	3.69	1.37	-1.37

Load Fixture and Strain Measurement

A specially designed load fixture is shown in Figure 2. External forces are applied through the four grips on top half of the fixture and measured with Sensotec Model 31BR load cells (range $\pm$444 N) attached to Sensotec Model GM signal conditioners. The four grips located on bottom half of specimen are stationary. Prior to placing the specimen within the fixture, an alignment jig was used to adjust the top four grips to a precise starting location such that the specimen would experience no forces upon initial placement in the fixture. The aluminum knobs shown in Figure 2b are rotated to generate a specified radial tensile force at that location. Multiple load configurations were used to create a series of different full-field strains for Q_{ij} evaluation.

The 24.5-cm-diameter specimen at eight locations 45° apart. Grips consisted of two small brass plates approximately 12 mm square. One plate had a threaded hole; the other a through-hole. A torque wrench was used to ensure uniform clamping pressure for each grip. Special care was used to prevent the top brass gripping plate from twisting and introducing undesirable stresses on the specimen.

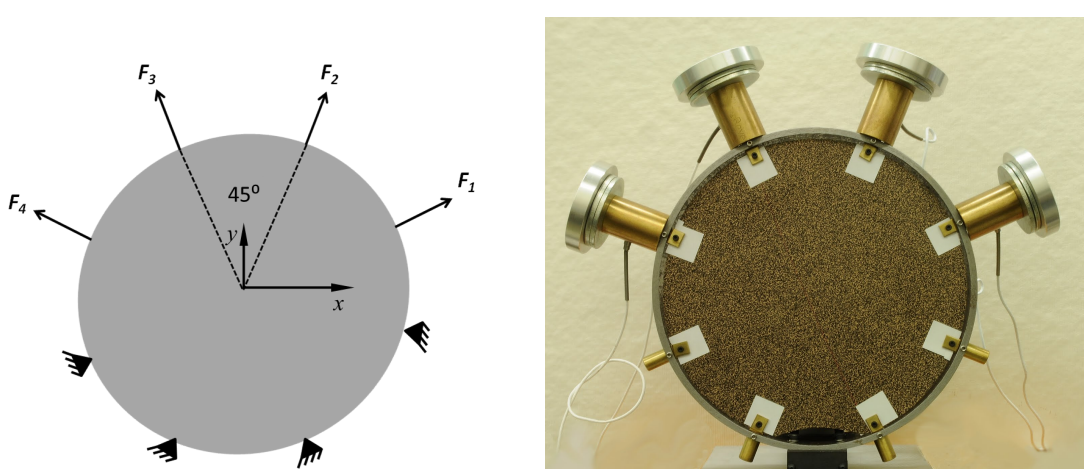

(a) Schematic of load fixture

(b) Actual load fixture

Figure 2: Load Fixture

Technique Used	Stereo Image Correlation
Camera	Allied Vision Technologies Stingray Model F504B
Lens	Computar M1614-MP2, 16 mm, f1.4
Lighting	Ambient florescent room lighting
Interface	IEEE 1394b - 800 Mb/s
Resolution	2452 x 2056
Sensor	Sony ICX655, CCD Progressive
Sensor Size	Type 2/3
Lens Mount	C
Field of View	38.7 cm x 32 cm
Facet Size	21 pixels, approx 3.3 mm x 3.3 mm
Software	Istra 4-D v2.1.5
Smoothing	7x7 adaptive polynomial

Table 3: DIC system components and parameters

The surface of the specimen was examined by a Dantec® DIC system whose details are listed in Table 3. Images were captured statically by waiting 5 minutes after load application was adjusted. A single reference image was used for each test.

The Virtual Fields Method

An abbreviated introduction to VFM is presented; the reader is encouraged to review the recent book [13] for a more thorough presentation. For a plane stress problem, the Principle of Virtual Work can be written as

$$\int_S (\sigma_1 \varepsilon_1^* + \sigma_2 \varepsilon_2^* + \sigma_6 \varepsilon_6^*)\, dS = \int_{L_f} \bar{T}_i u_i^* dl \tag{1}$$

where S is the area of 2-D domain, σ_i are stresses within S, u_i^* are kinematically admissible virtual displacements, ε_i^* are virtual strains associated with u_i^*, $\bar{T}_i$ are tractions applied on boundary of S, and L_f is the portion of S over which $\bar{T}_i$ are applied.

Assuming a linear elastic anisotropic material, the constitutive equation, using contracted index notation, is given by

$$\begin{Bmatrix} \sigma_1 \\ \sigma_2 \\ \sigma_6 \end{Bmatrix} = \begin{bmatrix} Q_{11} & Q_{12} & Q_{16} \\ Q_{12} & Q_{22} & Q_{23} \\ Q_{16} & Q_{26} & Q_{66} \end{bmatrix} \begin{Bmatrix} \varepsilon_1 \\ \varepsilon_2 \\ \varepsilon_6 \end{Bmatrix} \tag{2}$$

Substituting Equation 2 into Equation 1 gives

$$\begin{aligned} &\int_S Q_{11} \varepsilon_1 \varepsilon_1^* + \int_S Q_{22} \varepsilon_2 \varepsilon_2^* dS + \int_S Q_{12} (\varepsilon_1 \varepsilon_2^* + \varepsilon_2 \varepsilon_1^*)\, dS + \cdots \\ \cdots &+ \int_S Q_{16} (\varepsilon_1 \varepsilon_6^* + \varepsilon_6 \varepsilon_1^*)\, dS + \int_S Q_{26} (\varepsilon_2 \varepsilon_6^* + \varepsilon_2 \varepsilon_6^*)\, dS + \int_S Q_{66} \varepsilon_6 \varepsilon_6^* dS = \int_{L_f} \bar{T}_i u_i^* dl \end{aligned} \tag{3}$$

If the material is homogeneous, then each Q_{ij} is a constant and can be placed outside the integrals in Equation 3. In practice, six different u_i^* are used in Equation 3, one to identify each Q_{ij}. Special virtual fields simplify identification by choosing a u_i^* so that only one integral term exists on the left side of Equation 3. By approximating the integrals in Equation 3 as discrete summations, a system of linear equations is developed whose solution requires minimal computation. DIC provides information on each ε_i throughout specimen surface and load cells provide values for each $\bar{T}_i$.

Creation of virtual fields is accomplished by definition of a mesh of 4-node quadrilateral isoparametric elements, as shown in Figure 3. In order to have a kinematically admissible virtual field, grip nodes are virtually fixed in both u and v displacement because they correspond to stationary grips in Figure 2a. Additionally, load grips are restricted to radial displacement corresponding to forces F_4, F_3, F_2 and F_1. VFM elements in Figure 3 are not precisely rectangular as some asymmetry of grip and force locations was created during fabrication. VFM meshes are not required to conform to specimen boundaries. Some VFM elements lie completely outside the specimen area, S, while other elements straddle the external boundary of S. Only terms in Equation 3 with nonzero, experimentally-measured ε_i have a contribution to stiffness evaluation. Considine et al. [14] used this same load fixture for VFM stiffness identification and found 49 VFM elements were sufficient.

An important part of this analysis was to characterize the sensitivity of the identification process to strain noise. For this work we have extended the VFM process to reduce the sensitivity of noise on parameter identification to include Q_{16} and Q_{26}.

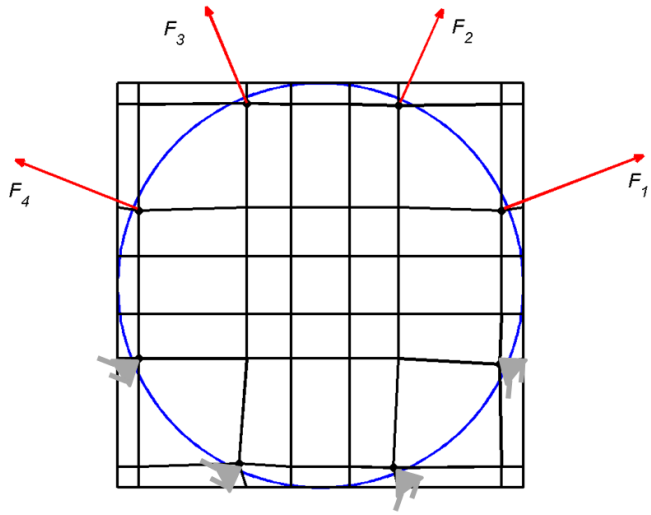

Figure 3: 49 element virtual mesh

We follow the noise reduction procedure given by [13] and use the term η_{ij}/Q_{ij} to characterize the variation of each identified stiffness. The term η_{ij}/Q_{ij} will usually be abbreviated to η_{ij}.

We take advantage of the knowledge that the Superposition Principle is valid for Equation 3 anticipating that some specimen loadings may better identify particular Q_{ij}, as determined by comparison of their η_{ij}. By tracking and combining the best specimen loadings a new composite identification can be performed.

Results and Discussion

Due to the multiaxial stresses intentionally created in the load fixture a stress vs. strain profile is not possible. Figure 4 shows normalized force and ε^c for each material, where norm refers to the 2-norm, ε^c is a composite strain given by Equation 4 and n is number of data points. The strain offset is an artifact of strains in the reference image for each test. Sufficient strains must be developed for reasonable parameter identification. Strain in Figure 4 suggests that identification may be difficult for smaller applied forces, e.g. Material A did not have significant change in strain until Test 4 at approximately 400 N. Material O, Test 7 had lower ε^c than for Test 6 even with increased applied forces; quality of parameter identification for Test 7, and other tests, will be examined subsequently.

$$\varepsilon^c = \frac{1}{3n}\sum_{i=1}^{n}\sqrt{\varepsilon_1^2+\varepsilon_2^2+\varepsilon_6^2} \tag{4}$$

Table 4 shows parameter identification for 'acceptable' tests of each material. Criteria for acceptance were:

- Q_{ij} must converge in less than 20 iterations. All tests in Table 4 converged in less than 10 iterations, i.e. this criterion eliminated no tests.
- η_{11}/Q_{11} and η_{22}/Q_{22} must be less than 200. In Table 4 η_{ij}/Q_{ij} has been shortened to η_{ij}. The value '200' was chosen based on review of Figure 4 and review of identification and allowed retention of an equal number of tests for each material.
- $(\eta_{12}/Q_{12})/(\eta_{11}/Q_{11})$ and $(\eta_{12}/Q_{12})/(\eta_{22}/Q_{22})$ must be less than 10. This criterion reflects the general difficulty of Q_{12} experimental identification.

Criteria for acceptance eliminated the first three load applications for each material. No increasing or decreasing trend exists for Q_{ij} identification for each material, suggesting the materials remained linear elastic. The η_{ij} tended to decrease, for Q_{11}, Q_{22}, Q_{12} and Q_{66}, with increased applied force, which is expected given the speciality conditions imposed to solve Equation 3. For Material O η_{16} and η_{26} were quite large because identified Q_{16} and Q_{26} were very near zero. The largest η_{16} and η_{26} occurred for Test 8, which had the smallest Q_{16} and Q_{26}.

Identified Q_{11} and Q_{22} were lower than calculated Q_{11} and Q_{22}; identified Q_{66} is higher than calculated Q_{66} and identified Q_{12}, Q_{16} and Q_{26} were close to calculated Q_{12}, Q_{16} and Q_{26}. Because of the relative magnitude of Q_{11} and Q_{22} as compared to

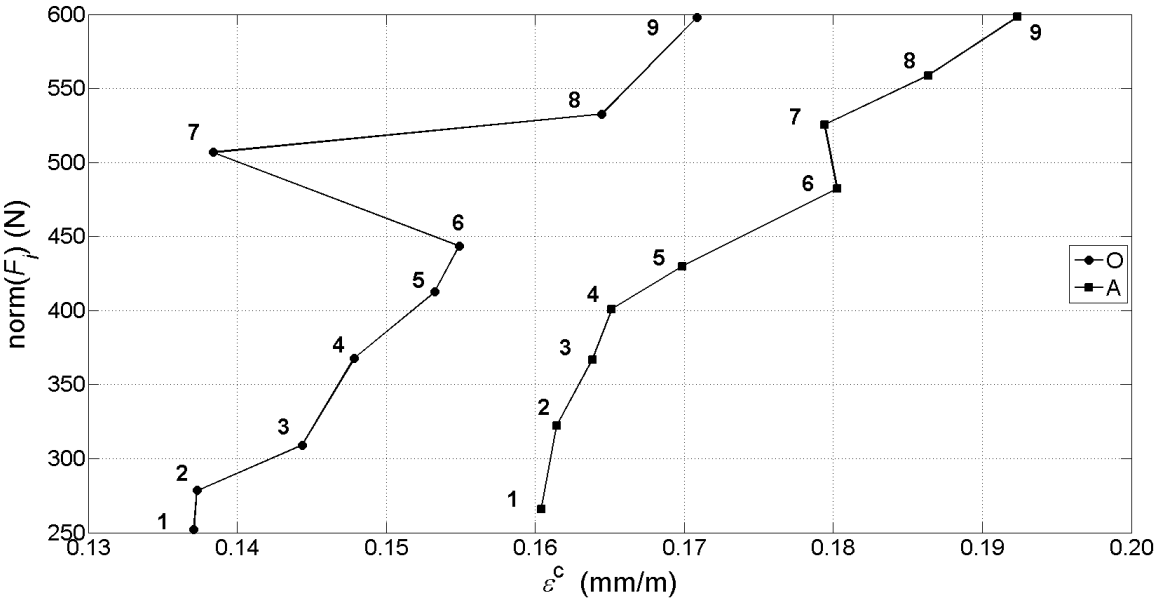

Figure 4: Examination of applied forces and induced strain for Materials O and A. Data labels refer to Test column in Table 4.

other Q_{ij} they had a greater influence on the procedure minimizing the effect of noise in the strain measurement on the VFM identification. For both materials COV for Q_{22} was large considering the 2-direction for each material was aligned vertically in Figure 2a which allowed development of larger ε_2. Tests 6 and 7 for Material O had identified Q_{22} closer to calculated Q_{22} and suggested that improvements in identification could be made. Similar η_{ij} for Q_{11}, Q_{22} and Q_{66} suggest the load fixture can make good parameter identification.

Figure 5 examines the linear elastic behavior of the material. No relationship existed between applied force and identified stiffnesses, noting that norm(Q_{ij}) is dominated by the largest Q_{ij}. Vertical dotted lines represent norms of calculated Q_{ij} (Table 2) for each material.

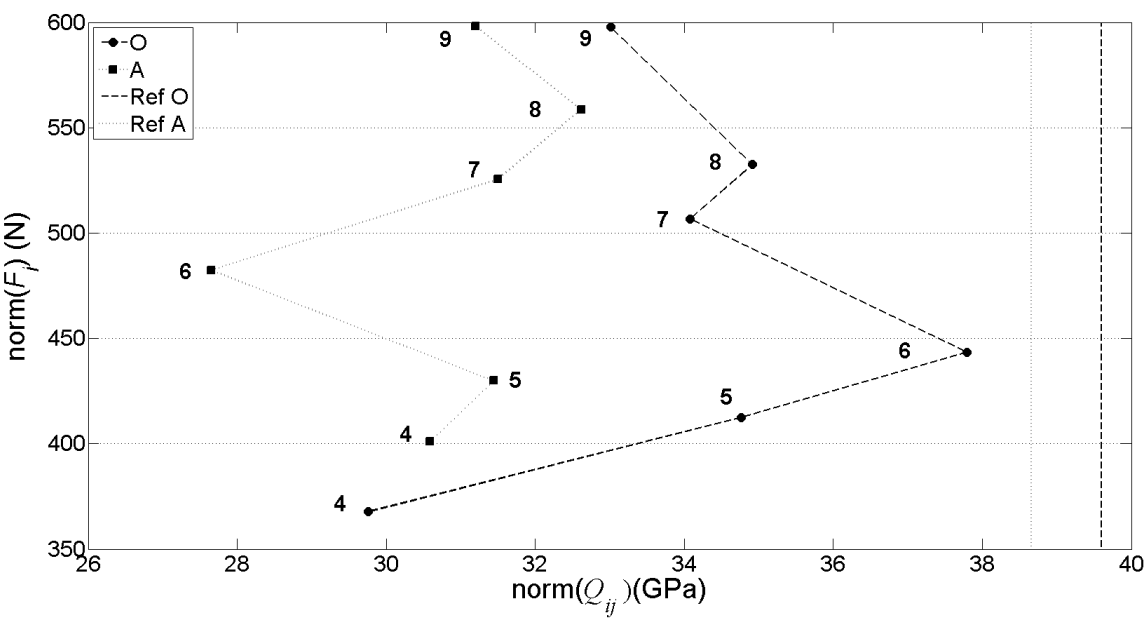

Figure 5: Relationship of applied forces and identified Q_{ij}. Reference Q_{ij} are from Table 2, Reference [11].

Table 4: Parameter identification using VFM mesh in Figure 3. η_{ij}/Q_{ij} has been shortened to η_{ij}. Q_{ij} units are GPa, η_{ij} units are m^3. Calculated Q_{ij} from Table 2 are repeated for convenience.

Material	Test	Q_{11}	Q_{22}	Q_{12}	Q_{66}	Q_{16}	Q_{26}	η_{11}	η_{22}	η_{12}	η_{66}	η_{16}	η_{26}
O	4	20.69	19.04	6.13	7.04	0.93	-2.65	181	164	520	215	1608	-519
	5	23.75	24.13	3.10	6.91	-1.81	1.09	198	163	1152	220	-972	1453
	6	24.49	27.71	4.23	6.36	-1.50	0.57	198	154	894	203	-1119	2539
	7	22.81	24.15	4.70	5.82	-0.32	1.36	140	131	615	164	-3383	796
	8	21.02	26.72	4.46	6.58	-0.12	0.35	131	131	632	151	-9009	3367
	9	21.45	23.75	4.12	6.98	0.29	-0.63	115	109	538	137	3368	-1553
	mean	22.37	24.25	4.46	6.62	-0.42	0.02						
	COV (%)	7.0	12.4	22.2	7.1	-249.7	9275.7						
	From [11]	27.84	27.84	3.06	2.90	N/A	N/A						
	From [12]	31.00	31.00	6.22	2.90	N/A	N/A						
A	4	20.94	21.29	2.85	5.23	1.78	-2.32	195	141	913	183	742	-495
	5	23.36	19.94	4.08	5.08	1.45	-1.09	177	128	653	155	784	-887
	6	20.45	17.23	2.95	5.43	3.05	-1.36	137	109	605	139	300	-616
	7	21.30	21.86	4.76	5.48	1.79	-2.13	135	116	463	138	518	-444
	8	23.12	21.63	3.54	6.16	1.79	-2.80	134	102	561	135	559	-323
	9	22.36	20.19	5.63	5.43	1.44	-1.39	119	96	334	122	560	-540
	mean	21.92	20.36	3.97	5.47	1.88	-1.85						
	COV (%)	5.5	8.4	27.3	6.8	31.7	-36.2						
	From [11]	27.04	27.04	3.85	3.69	1.37	-1.37						
	From [12]	30.21	30.21	7.01	3.69	1.37	-1.37						

Parameter identification was improved by application of the Superposition Principle to the individual tests in Table 4. A composite test was created by addition of applied forces and resulting strains for four consecutive tests producing a total of three composite tests for each material. Table 5 shows the results for parameter identification for composite tests. Direct comparison of η_{ij} requires more detail than can be provided here. The roughly four-fold decrease η_{ij} is expected because four tests were used in each composite test. Identified Q_{22} and Q_{12} for Material O were closer to their calculated values. Low values for Q_{11} may be attributed to orientation of specimen in the load fixture. For both materials the 1-direction was bracketed by a loading grip and a stationary grip, while the 2-direction was bracketed by loading grips. We expect improvement in identified Q_{11} through rotation of specimen by 45° such that both principal material directions are bracketed by loading grips. While the lower COV for each Q_{ij} can be partially attributed to fewer tests, i.e. three values for each Q_{ij} in the composite tests and six values in the individiual tests, some reduction is due to improved accuracy of the parameter identification.

Conclusion

This work introduced a novel load fixture designed to determine the anisotropic stiffnesses of a composite material using VFM. DIC was used to measure full-field strains under several different multi-axial load configurations. The Superposition Principle was incorporated due to large COV of identified stiffnesses and η_{ij}/Q_{ij} for single test analysis. Combined tests produced parameter identification with smaller COV and improved accuracy.

Table 5: Parameter identification using Superposition Principle and VFM mesh in Figure 3. η_{ij}/Q_{ij} has been shortened to η_{ij}. Q_{ij} units are GPa, η_{ij} units are m^3.

Material	Tests	Q_{11}	Q_{22}	Q_{12}	Q_{66}	Q_{16}	Q_{26}	η_{11}	η_{22}	η_{12}	η_{66}	η_{16}	η_{26}
O	4+5+6+7	23.01	26.02	3.66	6.27	-0.57	-0.70	46	40	248	50	-632	-498
	5+6+7+8	23.75	27.06	3.53	6.26	-0.50	0.71	41	37	250	46	-677	478
	6+7+8+9	22.21	25.33	4.26	6.51	-0.53	0.72	36	33	171	41	-554	411
	mean	22.99	26.14	3.82	6.35	-0.53	0.24						
	COV (%)	3.4	3.3	10.2	2.2	-6.8	337.37						
A	4+5+6+7	22.53	21.31	3.56	5.54	2.14	-1.32	41	32	181	38	133	-201
	5+6+7+8	23.09	21.70	3.48	5.59	2.20	-1.83	37	30	171	37	119	-137
	6+7+8+9	22.29	22.23	3.94	5.82	1.93	-2.19	34	28	141	34	127	-110
	mean	22.64	21.74	3.66	5.65	2.09	-1.78						
	COV (%)	1.82	2.12	6.82	2.68	6.77	-24.41						

References

[1] T. Pike, M. McArthur, and D. Schade, "Vacuum assisted resin transfer molding of a layered structural laminate for application on ground combat vehicles," *International SAMPE Technical Conference*, vol. 28, pp. 374 –380, 1996.

[2] J. W. J. Monib A. M.; Gillespie, "Damage tolerance of composite laminates subjected to ballistic impact," *Proceedings of ANTEC 98*, 14631467, 1998.

[3] X. Huang, J. W. Gillespie Jr, and T. Bogetti, "Process induced stress for woven fabric thick section composite structures," *Composite structures*, vol. 49, no. 3, pp. 303–312, 2000.

[4] K. Bernetich, J. Gillespie Jr, and B. Fink, "Improved damage tolerant integral armor via stitching and co-injection resin transfer molding," *Proceedings of the American Society for Composites Thirteenth Technical Conference, Baltimore, MD*, pp. 1491–1497, 1998.

[5] S. Abrate, "Impact on laminated composite materials," *Applied Mechanics Reviews*, vol. 44, no. 4, pp. 155–190, 1991.

[6] L. R. Holmes Jr., J. P. Wolbert, and J. M. Gardner, "A processing method for high fiber volume fraction composites," *International SAMPE Technical Conference*, Baltimore/Washington and Great Lakes Chapters, 2012.

[7] J. Ryder and F. W. Crossman, "A study of stiffness, residual strength and fatigue life relationships for composite laminates," DTIC Document, NASA CR-172211, Tech. Rep., 1983.

[8] M. Kinsella, D. Murray, D. Crane, J. Mancinelli, and M. Kranjc, "Mechanical properties of polymeric composites reinforced with high strength glass fibers," *International SAMPE Technical Conference*, vol. 33, pp. 1644–1657, 2001.

[9] "Sc-15: toughened epoxy resin system technical datasheet," Applied Poleramic Inc.: Benicia, CA, Tech. Rep., 2009.

[10] E. J. Rigas, T. J. Mulkern, S. M. Walsh, and S. P. Nguyen, "Effects of processing conditions on vacuum assisted resin transfer molding process (VARTM)," DTIC Document, ARL-TR-2480, Tech. Rep., 2001.

[11] B. D. Agarwal, L. J. Broutman, and K Chandrashekhara, *Analysis and performance of fiber composites*. Wiley, 2006.

[12] G. Staab, *Laminar Composites*. Butterworth-Heinemann, 1999.

[13] F. Pierron and M. Grédiac, *The Virtual Fields Method: Extracting Constitutive Mechanical Parameters from Full-Field Deformation Measurements*. Springer, 2012.

[14] J. Considine, F Pierron, K. Turner, and D. Vahey, "Anisotropy evaluation of paperboard with Virtual Fields Method," *Proceedings of SEM 2013 Annual Conference*, Paper 83, 2013.

LR Holmes Jr, JM Considine, F Pierron, KT Turner, "Anisotropy Characterization of Asymmetric Glass/Epoxy Composites,"Proceedings of 2013 Society of Experimental Mechanics Annual Conference, Paper 62, 2013.